Estimation of Volcanic Earthquakes at Kirishima Volcano Using Machine Learning

Yohei Yukutake[1], Ahyi Kim[2], and Takao Ohminato[1]

[1]Earthquake Research Institute
[2]Yokohama City University

April 4, 2023

Abstract

Volcanic earthquakes provide essential information for evaluating volcanic activity. As volcanic earthquakes are often characterized by swarm-like features, conventional methods using manual picking require much time in constructing seismic catalogs. In this study, using a machine learning framework and a trained model from a volcanic earthquake catalog, we obtained a detailed picture of volcanic earthquakes during the past 12 years at Kirishima volcano, southwestern Japan. We could detect earthquakes about 7.5 times larger than those in a conventional seismic catalog and obtain a high-resolution hypocenter distribution through waveform correlation analysis. Hypocenter clusters were estimated below the craters where magmatic or phreatic eruptions occurred in recent years. Increases in seismic activities, b-values, and low-frequency earthquakes were detected before the eruptions. The process can be carried out in real time, and monitoring volcanic earthquakes through machine learning contributes to understanding the changes in volcanic activity and improving eruption predictions.

Hosted file

959550_0_supp_10835538_rs60jh.docx available at https://authorea.com/users/559853/articles/632402-estimation-of-volcanic-earthquakes-at-kirishima-volcano-using-machine-learning

Estimation of Volcanic Earthquakes at Kirishima Volcano Using Machine Learning

Y. Yukutake[1], A. Kim[2], and T. Ohminato[1]

[1]Earthquake Research Institute, The University of Tokyo.

[2]Yokohama City University.

Corresponding author: Yohei Yukutake (yukutake@eri.u-tokyo.ac.jp)

Key Points:

- Using machine learning, earthquakes about 7.5 times larger than those in a conventional seismic catalog were detected.
- Hypocenter clusters were estimated below the craters where magmatic or phreatic eruptions occurred in recent years.
- Increases in seismic activities, *b*-values, and low-frequency earthquakes were detected before the eruptions.

Abstract

Volcanic earthquakes provide essential information for evaluating volcanic activity. As volcanic earthquakes are often characterized by swarm-like features, conventional methods using manual picking require much time in constructing seismic catalogs. In this study, using a machine learning framework and a trained model from a volcanic earthquake catalog, we obtained a detailed picture of volcanic earthquakes during the past 12 years at Kirishima volcano, southwestern Japan. We could detect earthquakes about 7.5 times larger than those in a conventional seismic catalog and obtain a high-resolution hypocenter distribution through waveform correlation analysis. Hypocenter clusters were estimated below the craters where magmatic or phreatic eruptions occurred in recent years. Increases in seismic activities, *b*-values, and low-frequency earthquakes were detected before the eruptions. The process can be carried out in real time, and monitoring volcanic earthquakes through machine learning contributes to understanding the changes in volcanic activity and improving eruption predictions.

Plain Language Summary

Volcanic earthquakes are caused by the migration of magma or hydrothermal fluid and changes in the stress field. This is an essential observation for predicting volcanic eruptions. However, the comprehensive detection of volcanic earthquakes and the estimation of accurate hypocenter locations involve many difficulties. The arrival time of seismic waves in waveform records must be picked to obtain reliable hypocenter parameters. On the other hand, phase picking based on visual inspection is time-consuming. In recent years, new phase-picking methods using machine learning techniques have been developed. In this study, we obtained a detailed picture of volcanic earthquakes during the past 12 years at Kirishima volcano, southwestern Japan, using a machine learning framework and a trained model from a volcanic earthquake catalog. We detected earthquakes about 7.5 times larger than those in the conventional seismic catalog and obtained a high-resolution hypocenter distribution through waveform correlation analysis. Hypocenter clusters were estimated below the craters where magmatic or phreatic eruptions occurred in recent years. Increases in seismic activities, *b*-values, and low-frequency earthquakes were detected before the eruption, which may reflect a precursive signal toward eruptions. Monitoring volcanic earthquakes through machine learning could thus contribute to improving our ability to perform eruption forecasting.

1 Introduction

Volcanic earthquakes are activated in response to the migration of magma or hydrothermal fluids (Hayashi & Morita, 2003; Kato et al., 2015; Shelly et al., 2013) or the changes in the stress field (Toda et al., 2002). They provide important information for evaluating volcanic activities (e. g., McNutt, 1996). For accurately evaluating the characteristics of earthquake activity, a precise seismic catalog must be constructed. The construction of an accurate seismic catalog on a real-time basis is also desirable for the improvement of eruption forecasting and hazard assessment. In the conventional procedures for constructing an earthquake catalog, an earthquake is detected using an indicator, such as the short-time to long-time ratio of waveform amplitude. Then, the arrival time and amplitude of the seismic phase are picked through visual inspection to obtain reliable hypocenter locations and magnitudes. Consequently, obtaining a precise seismic catalog takes an enormous amount of time.

In volcanic or geothermal regions, we often observe earthquake swarms during the activation of volcanic activity, where numerous volcanic earthquakes occur during a short period. As seismic waves from many events crowd into the waveform record with a short-time range, detecting earthquakes and phase picking is more complicated, even for expert researchers. In this regard, the matched filter method (e.g. Peng & Zhao, 2009; Shelly et al., 2007) is a powerful tool used to detect earthquakes for crowded waveform records. However, because this method involves cross-correlation analysis using waveforms of template earthquakes and continuous waveforms, detection is difficult when an earthquake occurs in a different location from the template earthquakes or when the waveform characteristics temporally change because of changes in focal mechanisms or surrounding medium, even in identical locations. Also, as the number of template earthquakes increases, the computational cost increases and real-time processing becomes more difficult.

Recently, automatic event detection and phase picking using machine learning have been developed (e. g.,Mousavi et al., 2020; Rossi et al., 2018; Zhu & Beroza, 2019). These methods reveal detailed pictures of seismicity that could not be obtained using conventional methods. For example, Ross et al. (2020) detected crustal earthquakes in Sothern California and revealed highly resolved fault structures from the hypocenter distribution and temporal change of the hypocentral area related to the migration of crustal fluid within fault zones. Meanwhile, Wilding et al. (2022) revealed the detailed structure of a sill complex at the deep part of the Hawai'i volcanic system using a high-resolution earthquake catalog with a machine learning procedure. In addition to phase picking, based on machine learning, reliable information on seismic activity could be estimated using clustering based on waveform similarity (Perol et al., 2018), the spatial pattern of wave propagation (Sugiyama et al., 2021), and classification of the seismic event type (Nakano et al., 2019).

Although the application of machine learning in monitoring seismic activity has been widely promoted, its application for volcanic regions is still challenging. One reason is that the existing trained models are created from the seismic catalog of ordinary earthquakes and may not fully reflect the characteristics of volcanic earthquakes. It is pointed out that applying optimally trained models matched to a target region improves the performance of detection and phase picking (Münchmeyer et al., 2022). Kim et al. (2022) constructed a deep learning model to detect seismic phase onset using a precise catalog of volcanic earthquakes at the Hakone volcano in central Japan and showed that the model improved the detection rate and accuracy of phase picking for volcanic earthquakes compared with the original trained model developed by Zhu and Beroza (2019), which they used as the starting model.

In this study, we applied the architecture of machine learning developed by Zhu and Beroza (2019) and the trained model by Kim et al. (2022) to seismic data from the Kirishima volcano and discussed its availability for monitoring volcanic earthquakes and the detailed picture of volcanic activity. The Kirishima volcanic complex is located in southern Kyushu, Japan and consists of approximately 20 volcanoes (Figure 1a). At Shinmoe-dake, small phreatic eruptions occurred in August 2008 and March–July 2010. A magmatic eruption after about 300 years (quasi-Plinian eruption) occurred in January 2011. Subsequently, magmatophreatic eruptions occurred again in October 2017, followed by a magmatic eruption on May 2018. A phreatic eruption also occurred at Iwo-Yama, located about 5 km northwest of Shinmoe-dake, in April 2018.

Several studies have reported the activity of volcanic earthquakes at Kirishima volcano based on a seismic catalog obtained using the conventional event detection method (Fukuoka District Meteorological Observatory and Kagoshima Local Meteorological Observatory, 2013; Yamada et al., 2015). However, the detailed spatial–temporal distribution of volcanic earthquakes and their relation to eruptive activities have not been fully clarified. Thus, we estimated a highly resolved hypocenter distribution based on phase-picking data using the machine learning method to obtain further information associated with volcanic activity. We also estimated a temporal change in *b*-values and event types using the frequency index.

2 Data and Methods

2.1 Seismic Observation

We used continuous waveform data from the past 12 years (2008–2019) recorded at 30 permanent stations installed in and around Kirishima volcano (Figure 1a) by the Earthquake Research Institute of the University of Tokyo (ERI), the Japan Meteorological Agency (JMA), the Research Institute for Earth Science and Disaster Resilience, and Kyushu University (Figure 1a). The average station spacing at Kirishima volcano is about 2 km. Broadband seismometers are installed at ERI stations, whereas short-period seismometers with a natural period of 1 Hz are installed at other stations. Seismic waveforms are continuously recorded at 100-Hz sampling intervals at all stations.

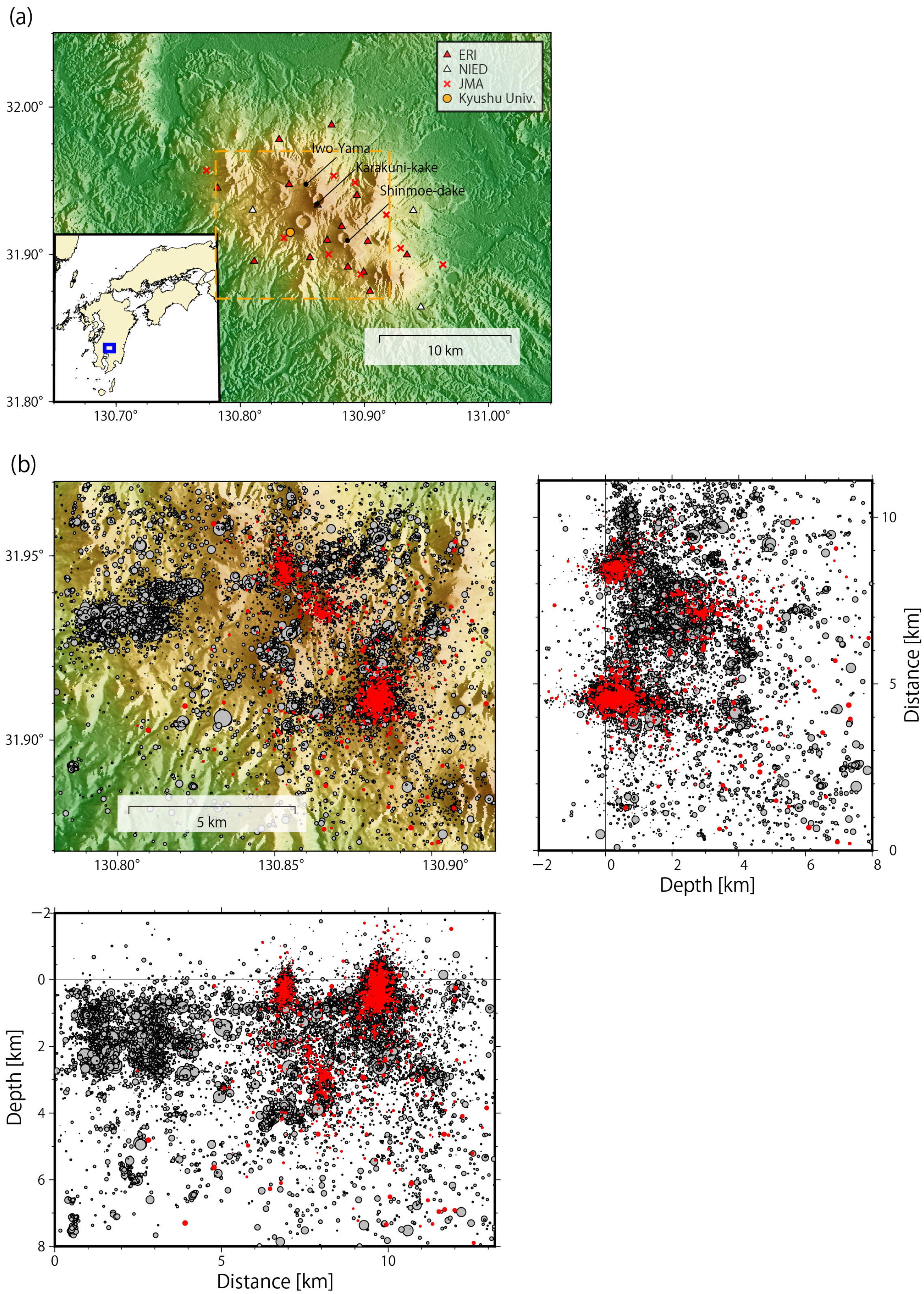

Figure 1. Map and seismicity at the Kirishima volcano. (a) Map of Kirishima volcano showing the locations of permanent seismic stations. The inset shows the target regions with respect to the

western part of the Japanese island. The orange rectangle corresponds to that shown in (b). (b) Hypocenter distribution of earthquakes beneath Kirishima volcano for the hypocenter catalog based on machine learning. The top panel shows the epicentral distribution, and the right and bottom panels indicate the depth distribution along the N–S and E–W sections, respectively. The depth of 0 km corresponds to the sea level. The red circles show the locations of low-frequency earthquakes classified based on the frequency index.

2.2 Phase Picking and Hypocenter Determination

We conducted the following processing for every hour of continuous waveform recording. The continuous waveform recordings were preprocessed by removing the offset and trend and then applying a 1-Hz high-pass filter to reduce the contamination of low-frequency noise. For the waveform record at each station, phase picking was performed using the PhaseNet architecture developed by Zhu and Beroza (2019) with a trained model by Kim et al. (2022). This trained model was created based on the seismic catalog of approximately 30,000 volcanic earthquakes at Hakone volcano over the past 20 years. The probability threshold for identifying *P*- and *S*-wave onsets was set at 0.3. The phase association was conducted using the REAL code developed by Zhang et al. (2019) for the *P*- and *S*-wave arrival times picked by PhaseNet. The threshold for identification of the same event was set at ≥3 stations for *P* waves and ≥2 stations for *S* waves. The theoretical arrival time from an assumed source to each station during the phase association was calculated using the 1D velocity structure beneath Kirishima volcano that has been used for the routine hypocenter determination at Kirishima Volcano Observatory of ERI (Mikada, 1996). For the picking data identified as seismic phases from the same event by the REAL code, the hypocenter was determined using the method of Hirata and Matsu'ura (1987), and the local magnitude was determined using the maximum amplitude following the empirical relation by Watanabe (1971). The hypocenter locations of 61200 earthquakes were estimated over 12 years.

We improved the original 1D velocity structure (Mikada, 1996) and estimated station corrections using the JHD method (Kissling et al., 1994) to obtain reliable absolute locations of earthquakes. In this analysis, we used earthquakes with at least eight phase pickings of both *P* and *S* waves obtained by the above procedure. With the estimated 1D velocity structure and station corrections (Figure S1), the hypocenter was determined using the hypomh_ps code (Kawanishi et al., 2009), only for the earthquake with at least four phase pickings of both *P* and *S* waves. We obtained the initial hypocenters of 55780 events.

We relocated the hypocenters using the double-difference (DD) method (Waldhauser & Ellsworth, 2000). In addition to the relative arrival time data (catalog data) obtained by PhaseNet, we also used relative travel time data through waveform correlation analysis (cross-correlation data). The waveforms within a time window of 0.1 s before and 0.4 s after the *P*- or *S*-wave arrival times were used for the correlation processing. For the stations where picking data were not available, the waveforms were trimmed based on the theoretical arrival time using the time window with the same length. We used the cross-correlation data with a cross-correlation coefficient ≥0.8. Consequently, 4.6 million station pairs for the catalog data and 12.5 million station pairs for the cross-correlation data were applied to the DD method. During the relocation process by the DD method, earthquakes with large travel time residuals or determined in air depth were eliminated. After applying the DD method, the locations of 40296 events were finally obtained (we call this hypocenter catalog the ML catalog).

2.3 *b*-values

We estimated the temporal variation of *b*-values for the earthquakes beneath Shinmoe-dake and Iwo-Yama using the ZMAP code (Wiemer & Wyss, 2000). The *b*-value is defined by the following equation.

$$\log N = a - bM. \quad (1)$$

Earthquakes were selected using a time window containing 300 events, moving the time window with an 83% overlap. The seismic catalog was split before and after the occurrence time of the eruptions to avoid mixing preseismicity and postseismicity data for the eruption. Meanwhile, because the number of earthquakes beneath Shinmoe-dake was limited before the 2011 eruption, we did not split the data during this eruption. For each time window, the completeness magnitudes (M_c) were calculated using the method of Wiemer and Wyss (2002). The *b*- and *a*-values in equation (1) were estimated, using the earthquakes that meet the condition of $M \geq M_c$. Then, we used the maximum likelihood estimate (Aki, 1965) for the estimation of the *b*- and *a*-values. The estimation of the b-value is detailed in Text S1.

2.4 Frequency Index

We classified the type of seismic signal on the basis of the frequency index (FI). Examples of spectra for volcano-tectonic and low-frequency earthquakes (defined by A- and B-type earthquakes, respectively, following the definition of Minakami (1974)) labeled in the seismic catalog by JMA (Figures S2, S3, and S4) are shown in Figure S5. The JMA catalog was obtained using manually picked data. Low-frequency earthquakes had a significant amplitude in the frequency range of 1–4 Hz compared with those of volcano-tectonic earthquakes. Therefore, for classifying these events, we defined the ratio of the average amplitude between 1–4 Hz and 10–15 Hz in the amplitude spectrum as FI. We could estimate FI for 26966 events. The estimation of FI is detailed in Text S2.

3 Results

The hypocenter distribution of the ML catalog is shown in Figure 1b. For comparison, we also show the hypocenter distribution based on the JMA catalog in Figure S2. We also show the time–depth distribution and cumulative number of earthquakes beneath the Kirishima volcano in Figure 2. Clusters of volcanic earthquakes were identified beneath Shinmoe-dake, Iwo-Yama, and in the western part of Kirishima volcano. The features of hypocenter distribution on the large scale are not significantly different from those in the JMA catalog (Figures 2, 3, S2, and S3). However, the ML catalog revealed a detailed pattern of seismic activities associated with eruptive activities beneath Shinmoe-dake and Iwo-Yama. The magnitude–frequency distribution for the ML and JMA catalogs is shown in Figure S4. We obtained the hypocenters of volcanic earthquakes about 7.5 times larger than that in the JMA catalog through the machine learning.

The magnitude completeness was −0.8 for the ML catalog, whereas that of the JMA catalog was 0.0, indicating an improvement in the detectability of earthquakes.

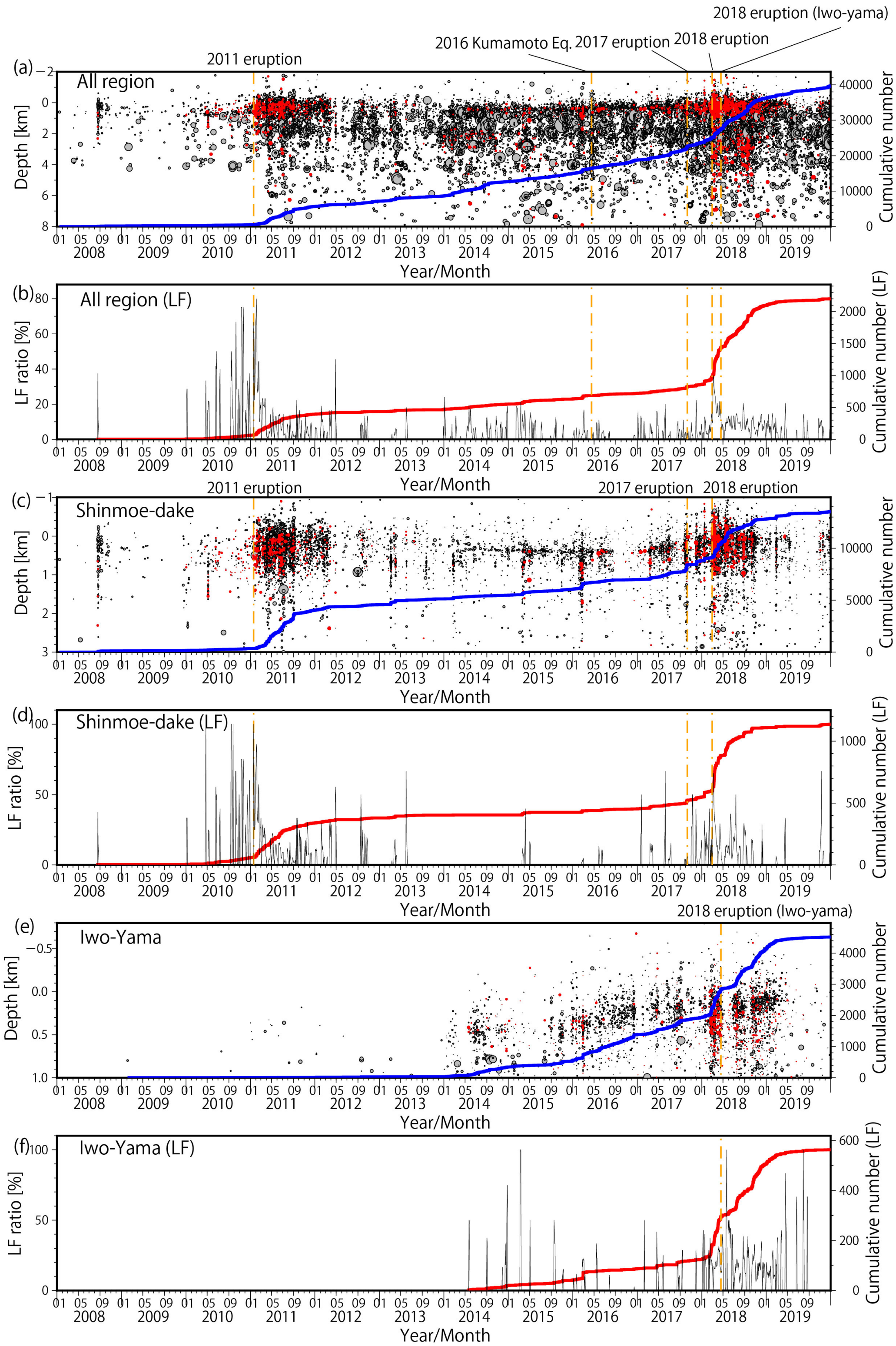

Figure 2. Depth–time distribution and the cumulative number of earthquakes. The red circles correspond to low-frequency (LF) earthquakes. The blue and red lines show the cumulative curve of volcanic and low-frequency earthquakes, respectively. The dotted vertical yellow lines show the occurrence time of main events: the 2011 Shinmoe-dake eruption, the 2016 Kumamoto earthquake, the 2017 and 2018 Shinmoedake-eruption, and the 2018 Iwo-yama phreatic eruption. (a) Whole region, (c) Shinmoe-dake, (e) Iwo-Yama. Panels (b), (d), and (f) show the cumulative curve of LF earthquakes and the ratio of LF earthquakes to volcano-tectonic earthquakes (thin black line) in each region. We used the time window of 7 days, moving at 2-day intervals, to estimate the LF ratio.

The seismic activity beneath Shinmoe-dake is shown in Figures 2c, 2d and 3a. Beneath Shinmoe-dake, numerous small volcanic earthquakes occurred in the depth range from −0.5 to 3 km below the crater (Depth of 0 km corresponds to sea level), showing a vertical hypocenter lineament that may reflect the magma pathway. At Shinmoe-dake, several eruptive events occurred: small phreatic eruptions on August 2008 and March–July 2010, a quasi-Plinian eruption on January 26, 2011, a magmatophreatic eruption on October 11, 2017, and a magmatic eruption on March 1, 2018. The seismic activity was gradually activated toward the 2011 magmatic eruption since 2010. The activity in the shallow part of the crater was also enhanced from March 2017 preceding the 2017 eruption. The upper depth of the seismicity area tended to gradually become shallower toward the 2017 eruption since March 2017 (Figure 2c). After the 2017 eruption, the seismic activity was quiescent for approximately 1 month. From December 2017, the earthquakes were activated again, showing a burst-like increment, leading to the 2018 eruption. The seismic activity remained high after the 2018 eruption until October 2018.

The seismic activity beneath Iwo-Yama is shown in Figures 2e, 2f and 3b. Volcanic earthquakes are concentrated in the depth range from −0.5 to 0.5 km beneath Iwo-Yama. A phreatic eruption occurred on April 19, 2018, at Iwo-Yama. In this area, seismic activity has increased since 2014. The upper depth limit of seismicity became shallower toward the 2018 eruption (Figure 2c). Moreover, before the eruption, seismic activity was remarkably activated since the end of February 2018. Seismic activity quiesced for a month after the eruption and activated again from late June 2018 through April 2019.

The temporal changes in the *b*-values within the two regions are shown in Figure 4. The *b*-values of earthquakes beneath Shinmoe-dake (Figure 4a) exceeded 1.2 before the 2011 eruption. After the 2011 eruption, *b*-values remained high, dropped temporarily, and again elevated at the end of 2011. The *b*-value rose again to a high value of 2 in early 2013 and then gradually declined through 2015, showing slight fluctuations. From the beginning of 2017, it increased again toward the 2017 eruption. After the eruption, the *b*-values increased again toward the 2018 magmatic eruption. Although the fitness for the Gutenberg–Richter law is not very good in the Iwo-Yama region (Figure 4b), the *b*-value increased through the beginning of 2016. After once dropping, we see an abrupt increase in the *b*-values just before the 2018 phreatic eruption at Iwo-Yama.

Low-frequency earthquakes concentrated on the area just beneath the crater of Shinmoe-dake and Iwo-Yama. Another cluster of low-frequency earthquakes was also identified at a depth of 3 km below Karakuni-dake (Figure 1b). The temporal sequence of seismicity shows that the number of low-frequency earthquakes just below the crater of Shinmoe-dake and Iwo-Yama increased before the eruptions (Figures 2d and 2f). From 2014 to 2015, the number of low-frequency earthquakes slightly increased (Figure 2b). Although the eruption did not occur during this period, an expansion of the GPS baseline length was observed (Kurihara et al., 2019), suggesting that the supply of magmatic fluid was activated.

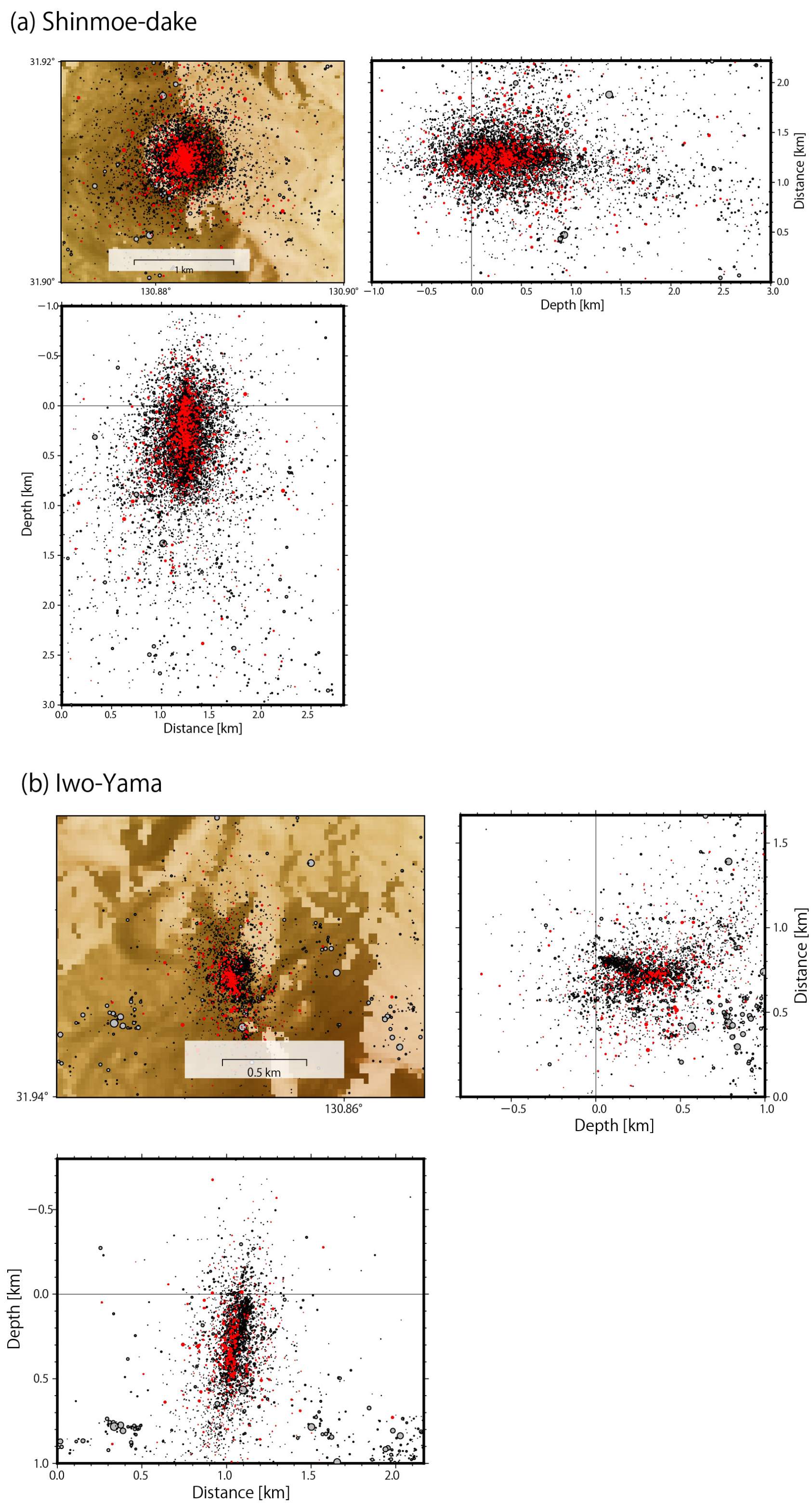

Figure 3. Hypocenter distributions beneath Shinmoe-dake and Iwo-yama. (a) Hypocenter distribution of earthquakes beneath Shinmoe-dake. (top) Epicentral distribution and (right and bottom) depth distributions along the N–S and E-W sections. Red circles correspond to the

hypocenters of low-frequency earthquakes. (b) Hypocenter distribution of earthquakes beneath Iwo-Yama.

4 Discussion and Conclusions

In this study, we developed a seismic catalog for the Kirishima volcano using automatic phase picking based on the machine learning framework. The resulting catalog was improved in terms of detectability compared with the JMA catalog based on manual phase picking (Figure S4). In this study, we obtained the detailed history of volcanic earthquakes at Kirishima volcano using the learning model derived from the hypocenter catalog at the different volcano, showing the applicability of the model. This model enables us to obtain seismic activity at volcanoes that have not been adequately developed seismic catalogs yet. Following the 2016 Kumamoto earthquake in the central part of Kyushu, numerous aftershocks occurred (e.g., Asano & Iwata, 2016). The seismicity beneath Kirishima volcano did not change for both seismic catalogs (Figures 2a, S3). This result implies that event detection based on machine learning has hardly caused any false detections even if the waveforms were contaminated by wave trains from outside of the study area.

We compared the seismic catalog derived from the original learning model developed by Zhu and Beroza (2019) from 2017 to 2019 to evaluate the performance of the trained model based on volcanic earthquakes (Kim et al., 2022) (Figure S7). Although the main characteristics of hypocenter distributions were not significantly different between the two catalogs, we can detect about 16% more earthquakes using the learning model derived from volcanic earthquakes compared with the original learning model, suggesting an improvement in the detectability in volcanic regions.

The highly resolved seismic catalog provides important information that may correspond to precursive signals toward eruptions. We detected the activation of volcanic earthquakes before the eruptions at Shinmoe-dake and Iwo-Yama (Figure 2). The 2017 and 2018 eruptions at Shinmoe-dake occurred when the *b*-values were close to 1.5 (Figure 4a). We also observed the abrupt increase in the *b*-value before the 2018 eruption at Iwo-Yama (Figure 4b). The high *b*-values observed during fluid-induced seismicity are interpreted as reflecting a low shear stress level on fault planes (Mukuhira et al., 2021). The activation of volcanic earthquakes with the increment of the *b*-values is caused by an elevation of magmatic fluid pressure (Nanjo et al., 2018). The high *b*-values with the increment of seismic activity before an eruption (Figures 2 and 4) may reflect unstable conditions in and around a volcanic conduit due to the increment of fluid pressure accompanied by the supply of magma. Meanwhile, as enough earthquakes were not obtained before the 2011 eruption at Shinmoe-dake, the detailed temporal sequence of *b*-values preceding the 2011 eruption could not be discussed in this study.

We also detected the activation of low-frequency earthquakes before the 2011, 2017, and 2018 eruptions at Shinmoe-dake (Figure 2d). The increment of the ratio of low-frequency earthquakes to volcano-tectonic earthquakes before the eruptions may reflect the interaction between magmatic and shallow hydrothermal fluids (e.g., McNutt, 1996). The activation of low-frequency earthquakes at the deeper part of the volcano (deeper than 10 km) and crustal expansions due to an inflation of pressure source at the depth of 8 km were detected approximately 1 year before the 2011 eruptions, suggesting the supply of magma into the volcanic root (Kurihara et al., 2019; Nakao et al., 2013). The rapid increment of the ratio of low-frequency earthquakes since April 2010 suggests the supply of new magmatic fluid into the shallow part beneath the volcanic conduit. The expansion of the hypocenter area to the shallow region beneath Iwo-Yama since 2014 toward the 2018 phreatic eruption may reflect a gradual intrusion of hydrothermal fluid beneath the low-permeable cap structure developed in the shallow hydrothermal system (Tsukamoto et al., 2018).

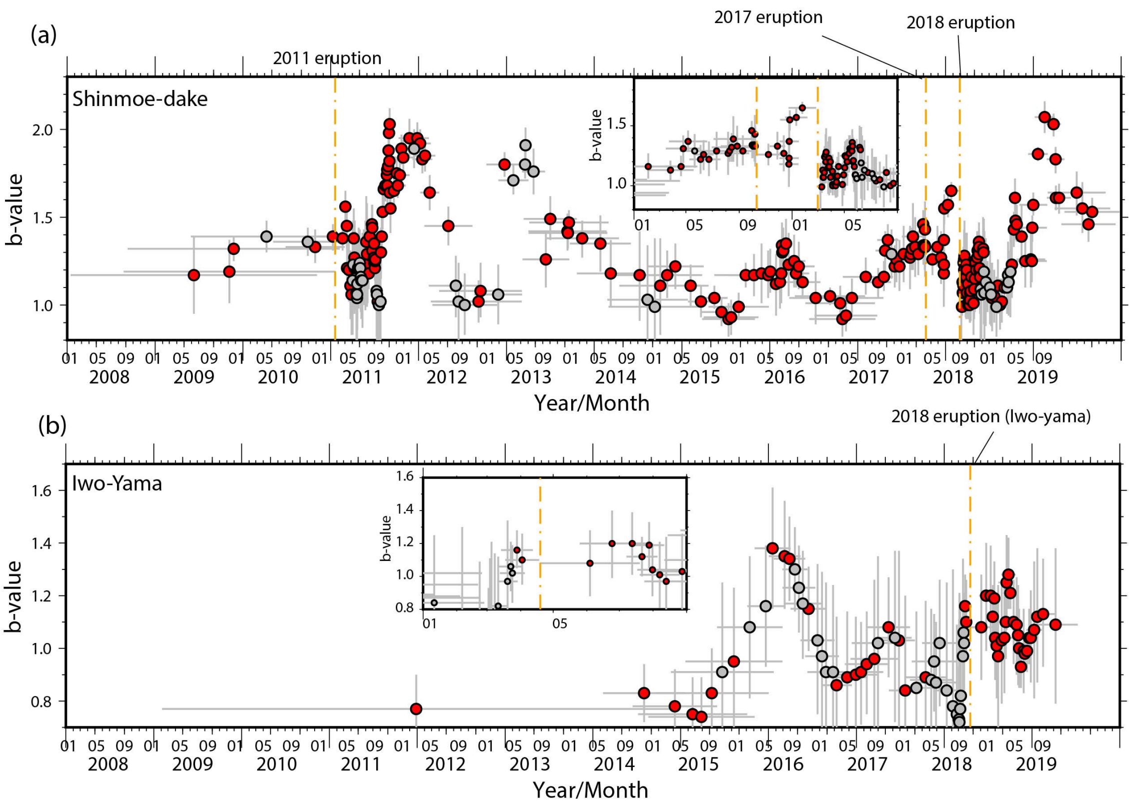

Figure 4. Temporal changes in *b*-values. (a) Shinmoe-dake and (b) Iwo-yama. The horizontal and vertical gray lines at each circle show the time window for selecting the earthquakes and the error bar of the *b*-value estimated using the bootstrap resampling method. Red circles represent reliable *b*-value estimations with residuals for the theoretical Gutenberg–Richter law distribution ≤10%. Inset diagrams in panels (a) and (b) show the magnified plot around the 2017 and 2018 eruptions at Shinmoe-dake and the 2018 eruption at Iwo-Yama, respectively.

Using the machine learning architecture developed by Zhu and Beroza (2019) and a trained model from the seismic catalog of the Hakone volcano (Kim et al., 2022), we obtained a high-quality seismic catalog of volcanic earthquakes at Kirishima volcano from 2008 to 2019. We could produce a seismic catalog with higher detectability than the conventional seismic catalog based on manual phase picking and could estimate the highly resolved hypocenter distribution through relative hypocenter relocation using wave cross-correlation analysis. From the seismic catalog, the activations of volcanic earthquakes and increment of *b*-values were detected preceding the magmatic and phreatic eruptions at Kirishima volcano. This improved detectability enables evaluating eruption risks through statistical analysis based on *b*-values and the temporal sequence of low-frequency earthquake activity, as well as the spatial–temporal sequence of volcanic earthquakes. Using a standard Linux machine, the computation time to obtain initial hypocenters for a 1-h waveform record is only a few minutes. Therefore, this system contributes to the improvement of our ability to perform eruption forecasting.

Acknowledgments

We used the seismic waveform data obtained by the Japan Meteorological Agency (JMA), the National Research Institute for Earth Science and Disaster Prevention, Kyushu University, and the Earthquake Research Institute of the University of Tokyo. JMA provided us with the hypocenter catalog of volcanic earthquakes. This research was supported by the Next Generation Volcano Research and Human Resource Development Project of the Ministry of Education, Culture, Sports, Science and Technology of Japan and a Grant-in-Aid for Scientific Research (C) (JSPS KAKENHI No. 22K03752).

Open Research

Data Availability Statement

The waveform data are obtainable from the web page of NIED Hi-net (National Research Institute for Earth Science and Disaster Resilience, 2019). The hypocenter catalog obtained in this study is available in the data repository (Yukutake, 2023). Most of the figures in the study were created with Generic Mapping Tools software (Wessel et al., 2019). The b-values were calculated using the ZMAP program (Wiemer, 2001).

References

Aki, K. (1965). Maximum likelihood estimate of b in the formula log N = a-bM and its confidence limits. *Bulletin of the Earthquake Research Institute, University of Tokyo, 43*, 237-239.

Asano, K., & Iwata, T. (2016). Source rupture processes of the foreshock and mainshock in the 2016 Kumamoto earthquake sequence estimated from the kinematic waveform inversion of strong motion data. *Earth, Planets and Space, 68*(1), 147. https://doi.org/10.1186/s40623-016-0519-9

Fukuoka District Meteorological Observatory and Kagoshima Local Meteorological Observatory. (2013). The 2011 Eruptive Activities of Shinmoedake Volcano, Kirishimayama, Kyushu, Japan. *Journal of Seismology, Volcanology and related Engineering (in Japanese with Englishu abstract), 77*, 65-96.

Hayashi, Y., & Morita, Y. (2003). An image of a magma intrusion process inferred from precise hypocentral migrations of the earthquake swarm east of the Izu Peninsula. *Geophysical Journal International, 153*(1), 159-174. http://dx.doi.org/10.1046/j.1365-246X.2003.01892.x

Hirata, N., & Matsu'ura, M. (1987). Maximum-likelihood estimation of hypocenter with origin time eliminated using nonlinear inversion technique. *Physics of the Earth and Planetary Interiors, 47*(0), 50-61. http://www.sciencedirect.com/science/article/pii/0031920187900665

Kato, A., Terakawa, T., Yamanaka, Y., Maeda, Y., Horikawa, S., Matsuhiro, K., & Okuda, T. (2015). Preparatory and precursory processes leading up to the 2014 phreatic eruption of Mount Ontake, Japan. *Earth, Planets and Space, 67*(1), 1-11.

Kawanishi, R., Iio, Y., Yukutake, Y., Shibutani, T., & Katao, H. (2009). Local stress concentration in the seismic belt along the Japan Sea coast inferred from precise focal mechanisms: Implications for the stress accumulation process on intraplate earthquake faults. *Journal of Geophysical Research, 114*(B1).

Kim, A., Nakamura, Y., Yukutake, Y., Uematsu, H., & Abe, Y. (2022). Seismic wave detection at Hakone volcano using machine learning: Toward improving the detection accuracy when there are multiple seismic waves in the same time window. *Abstracts of Japan Geoscience Union Meeting 2022*, SCG51-P05.

Kissling, E., Ellsworth, W. L., Eberhart-Phillips, D., & Kradolfer, U. (1994). Initial reference models in local earthquake tomography. *Journal of Geophysical Research: Solid Earth, 99*(B10), 19635-19646. http://dx.doi.org/10.1029/93JB03138

Kurihara, R., Obara, K., Takeo, A., & Tanaka, Y. (2019). Deep Low-Frequency Earthquakes Associated With the Eruptions of Shinmoe-dake in KirishimaVolcanoes. *Journal of Geophysical Research: Solid Earth, 124*(12), 13079-13095. https://agupubs.onlinelibrary.wiley.com/doi/abs/10.1029/2019JB018032

Münchmeyer, J., Woollam, J., Rietbrock, A., Tilmann, F., Lange, D., Bornstein, T., et al. (2022). Which Picker Fits My Data? A Quantitative Evaluation of Deep Learning Based Seismic Pickers. *Journal of Geophysical Research: Solid Earth, 127*(1), e2021JB023499. https://agupubs.onlinelibrary.wiley.com/doi/abs/10.1029/2021JB023499

McNutt, S. R. (1996). Seismic Monitoring and Eruption Forecasting of Volcanoes: A Review of the State-of-the-Art and Case Histories. In R. Scarpa & R. I. Tilling (Eds.), *Monitoring and Mitigation of Volcano Hazards* (pp. 99-146). Berlin, Heidelberg: Springer Berlin Heidelberg.

Mikada, H. (1996). A Seismic Reflection Analysis on Refraction Data from the 1994 Kirishima Explosion Experiment. *BULLETIN OF THE VOLCANOLOGICAL SOCIETY OF JAPAN, 41*(4), 159-170.

Minakami, T. (1974). Chapter 1 - Seismology of Volcanoes in Japan. In L. Civetta, P. Gasparini, G. Luongo, & A. Rapolla (Eds.), *Developments in Solid Earth Geophysics* (Vol. 6, pp. 1-27): Elsevier.

Mousavi, S. M., Ellsworth, W. L., Zhu, W., Chuang, L. Y., & Beroza, G. C. (2020). Earthquake transformer—an attentive deep-learning model for simultaneous earthquake detection and phase picking. *Nature Communications, 11*(1), 3952. https://doi.org/10.1038/s41467-020-17591-w

Mukuhira, Y., Fehler, M. C., Ito, T., Asanuma, H., & Häring, M. O. (2021). Injection-Induced Seismicity Size Distribution Dependent on Shear Stress. *Geophysical Research Letters, 48*(8), e2020GL090934. https://agupubs.onlinelibrary.wiley.com/doi/abs/10.1029/2020GL090934

Nakano, M., Sugiyama, D., Hori, T., Kuwatani, T., & Tsuboi, S. (2019). Discrimination of Seismic Signals from Earthquakes and Tectonic Tremor by Applying a Convolutional Neural Network to Running Spectral Images. *Seismological Research Letters, 90*(2A), 530-538. https://doi.org/10.1785/0220180279

Nakao, S., Morita, Y., Yakiwara, H., Oikawa, J., Ueda, H., Takahashi, H., et al. (2013). Volume change of the magma reservoir relating to the 2011 Kirishima Shinmoe-dake eruption—Charging, discharging and recharging process inferred from GPS measurements. *Earth, Planets and Space, 65*(6), 3. https://doi.org/10.5047/eps.2013.05.017

Nanjo, K. Z., Miyaoka, K., Tamaribuchi, K., Kobayashi, A., & Yoshida, A. (2018). Related spatio-temporal changes in hypocenters and the b value in the 2017 Kagoshima Bay swarm activity indicating a rise of hot fluids. *Tectonophysics, 749*, 35-45. http://www.sciencedirect.com/science/article/pii/S0040195118303512

National Research Institute for Earth Science and Disaster Resilience. (2019). *NIED Hi-net, National Research Institute for Earth Science and Disaster Resilience*. Retrieved from: 10.17598/NIED.0003

Peng, Z., & Zhao, P. (2009). Migration of early aftershocks following the 2004 Parkfield earthquake. *Nature Geoscience, 2*(12), 877-881.

Perol, T., Gharbi, M., & Denolle, M. (2018). Convolutional neural network for earthquake detection and location. *Science Advances, 4*(2), e1700578. https://www.science.org/doi/abs/10.1126/sciadv.1700578

Ross, Z. E., Cochran, E. S., Trugman, D. T., & Smith, J. D. (2020). 3D fault architecture controls the dynamism of earthquake swarms. *Science, 368*(6497), 1357-1361. https://science.sciencemag.org/content/sci/368/6497/1357.full.pdf

Rossi, G., Fabris, P., & Zuliani, D. (2018). Overpressure and Fluid Diffusion Causing Non-hydrological Transient GNSS Displacements. *pure and applied geophysics, 175*(5), 1869-1888. https://doi.org/10.1007/s00024-017-1712-x

Shelly, D. R., Beroza, G. C., & Ide, S. (2007). Non-volcanic tremor and low-frequency earthquake swarms. *Nature, 446*(7133), 305-307. http://www.ncbi.nlm.nih.gov/pubmed/17361180

Shelly, D. R., Hill, D. P., & Massin, F. (2013). A fluid-driven earthquake swarm on the margin of the Yellowstone caldera. *Journal of Geophysical Research: Solid Earth, 118*. http://dx.doi.org/10.1002/jgrb.50362

Sugiyama, D., Tsuboi, S., & Yukutake, Y. (2021). Application of deep learning-based neural networks using theoretical seismograms as training data for locating earthquakes in the Hakone volcanic region, Japan. *Earth, Planets and Space, 73*(1), 135. https://doi.org/10.1186/s40623-021-01461-w

Toda, S., Stein, R. S., & Sagiya, T. (2002). Evidence from the AD 2000 Izu islands earthquake swarm that stressing rate governs seismicity. *Nature, 419*(6902), 58-61.

Tsukamoto, K., Aizawa, K., Chiba, K., Kanda, W., Uyeshima, M., Koyama, T., et al. (2018). Three-Dimensional Resistivity Structure of Iwo-Yama Volcano, Kirishima Volcanic Complex, Japan: Relationship to Shallow Seismicity, Surface Uplift, and a Small Phreatic Eruption. *Geophysical Research Letters, 45*(23), 12,821-812,828. https://agupubs.onlinelibrary.wiley.com/doi/abs/10.1029/2018GL080202

Waldhauser, F., & Ellsworth, W. L. (2000). A Double-Difference Earthquake Location Algorithm: Method and Application to the Northern Hayward Fault, California. *Bulletin of the Seismological Society of America, 90*(6), 1353-1368. http://www.bssaonline.org/content/90/6/1353.abstract

Watanabe, H. (1971). Determination of Earthquake Magnitude at Regional Distance in and near Japan. *Zisin (Journal of the Seismological Society of Japan. 2nd ser.), 24*(3), 189-200.

Wessel, P., Luis, J. F., Uieda, L., Scharroo, R., Wobbe, F., Smith, W. H. F., & Tian, D. (2019). The Generic Mapping Tools Version 6. *Geochemistry, Geophysics, Geosystems, 20*(11), 5556-5564. https://agupubs.onlinelibrary.wiley.com/doi/abs/10.1029/2019GC008515

Wiemer, S. (2001). A Software Package to Analyze Seismicity: ZMAP. *Seismological Research Letters, 72*(3), 373-382. https://dx.doi.org/10.1785/gssrl.72.3.373

Wiemer, S., & Wyss, M. (2000). Minimum Magnitude of Completeness in Earthquake Catalogs: Examples from Alaska, the Western United States, and Japan. *Bulletin of the Seismological Society of America, 90*(4), 859-869. http://dx.doi.org/10.1785/0119990114

Wiemer, S., & Wyss, M. (2002). Mapping spatial variability of the frequency-magnitude distribution of earthquakes. *Advances in geophysics, 45*, 259-302.

Wilding, J. D., Zhu, W., Ross, Z. E., & Jackson, J. M. (2022). The magmatic web beneath Hawai'i. *Science, 379*(6631), 462-468. https://www.science.org/doi/abs/10.1126/science.ade5755

Yamada, T., Yukutake, Y., Terakawa, T., & Arai, R. (2015). Migration of earthquakes with a small stress drop in the Tanzawa Mountains, Japan. *Earth, Planets and Space, 67*(1), 175. http://www.earth-planets-space.com/content/67/1/175

Yukutake, Y. (2023). Earthquake catalog of volcanic earthquake beneath the Kirishima volcano, southwest Japan. *figshare*. 10.6084/m9.figshare.22281403

Zhang, M., Ellsworth, W. L., & Beroza, G. C. (2019). Rapid Earthquake Association and Location. *Seismological Research Letters, 90*(6), 2276-2284. https://doi.org/10.1785/0220190052

Zhu, W., & Beroza, G. C. (2019). PhaseNet: a deep-neural-network-based seismic arrival-time picking method. *Geophysical Journal International, 216*(1), 261-273. https://doi.org/10.1093/gji/ggy423

Figure1.

(a)

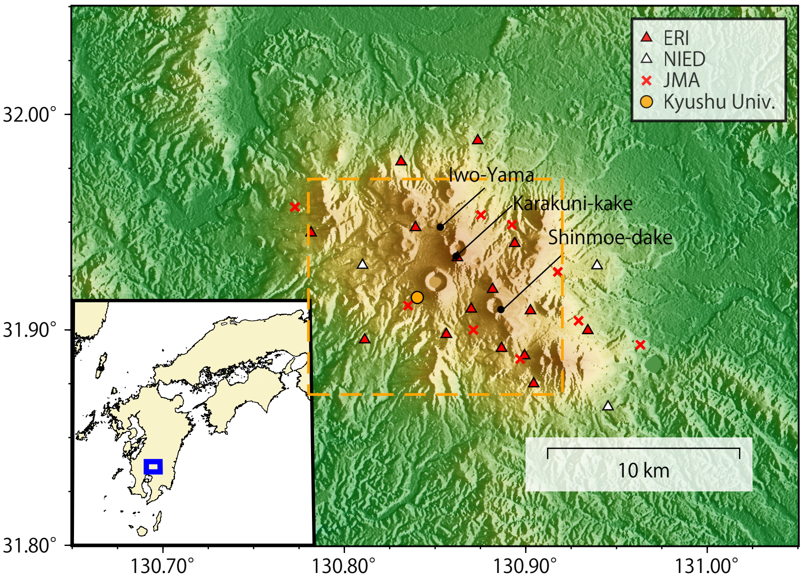
ERI
NIED
JMA
Kyushu Univ.
Iwo-Yama
Karakuni-kake
Shinmoe-dake
10 km
32.00°
31.90°
31.80°
130.70°
130.80°
130.90°
131.00°

(b)

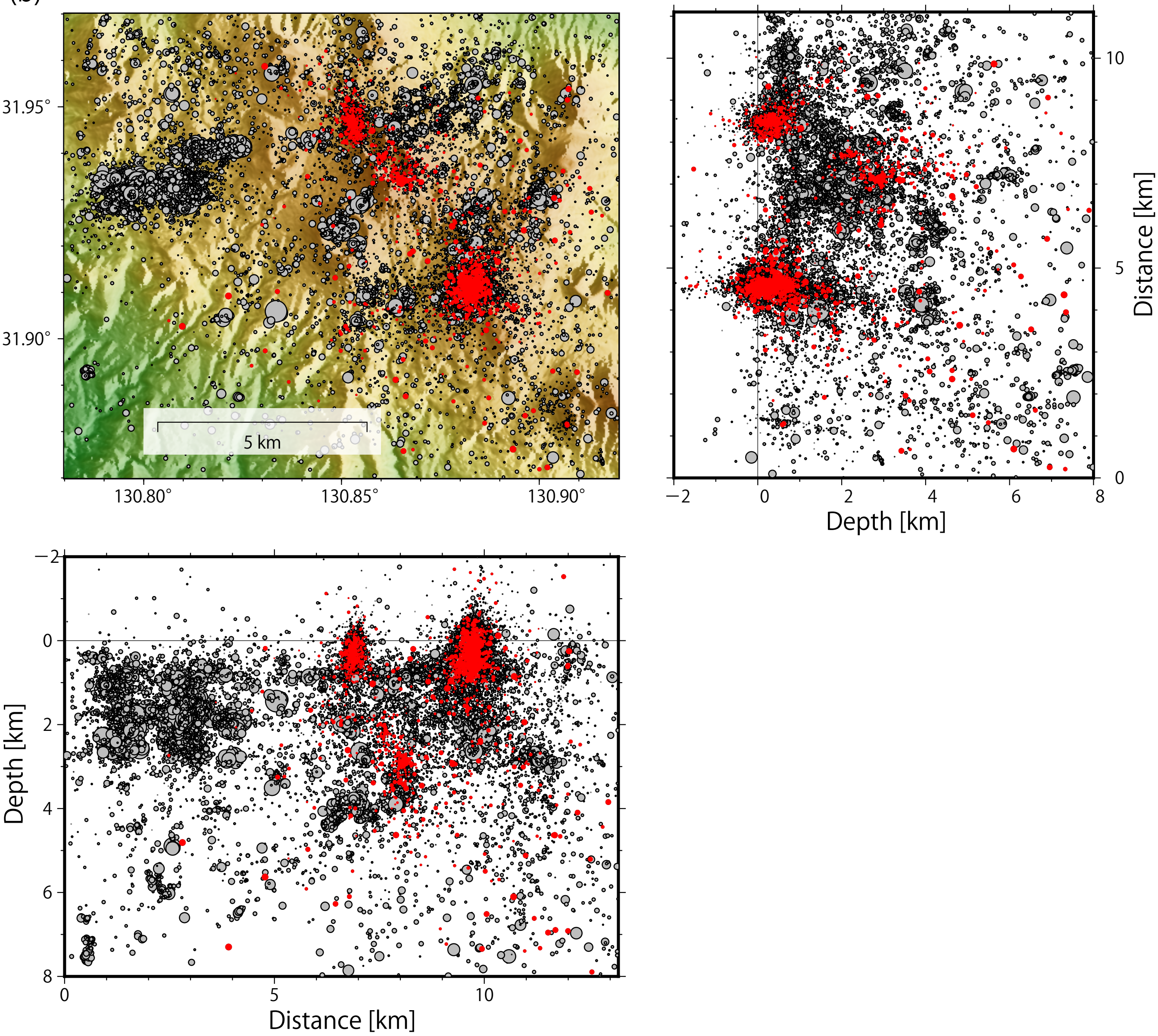
31.95°
31.90°
5 km
130.80°
130.85°
130.90°
Distance [km]
Depth [km]
−2
0
2
4
6
8
10
5
0

Figure2.

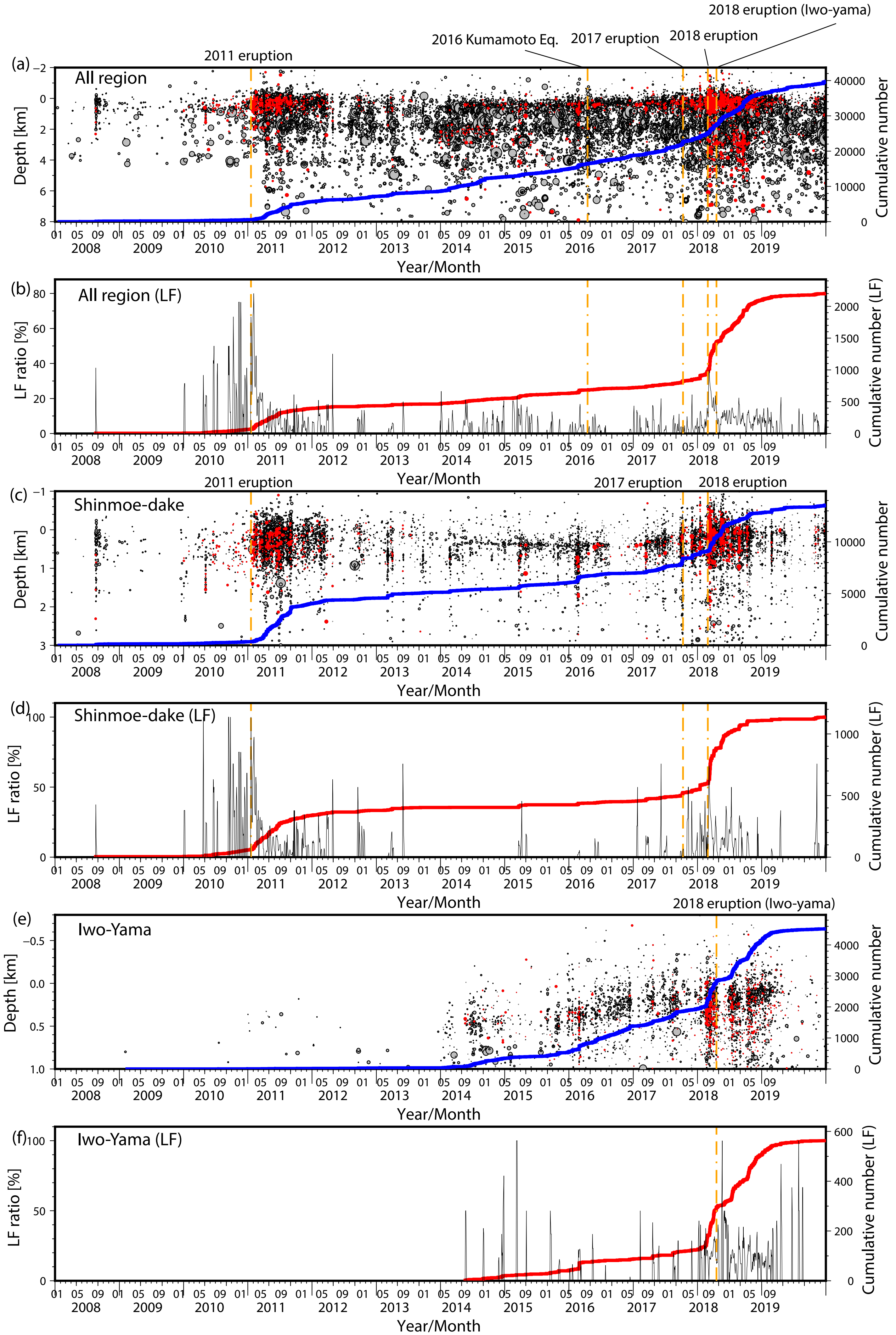

2018 eruption (Iwo-yama)
2016 Kumamoto Eq.
2017 eruption
2018 eruption
2011 eruption
(a)
All region
Depth [km]
Cumulative number
Year/Month
(b)
All region (LF)
LF ratio [%]
Cumulative number (LF)
Year/Month
(c)
Shinmoe-dake
2011 eruption
2017 eruption
2018 eruption
Depth [km]
Cumulative number
Year/Month
(d)
Shinmoe-dake (LF)
LF ratio [%]
Cumulative number (LF)
Year/Month
(e)
Iwo-Yama
2018 eruption (Iwo-yama)
Depth [km]
Cumulative number
Year/Month
(f)
Iwo-Yama (LF)
LF ratio [%]
Cumulative number (LF)
Year/Month

Figure3.

(a) Shinmoe-dake

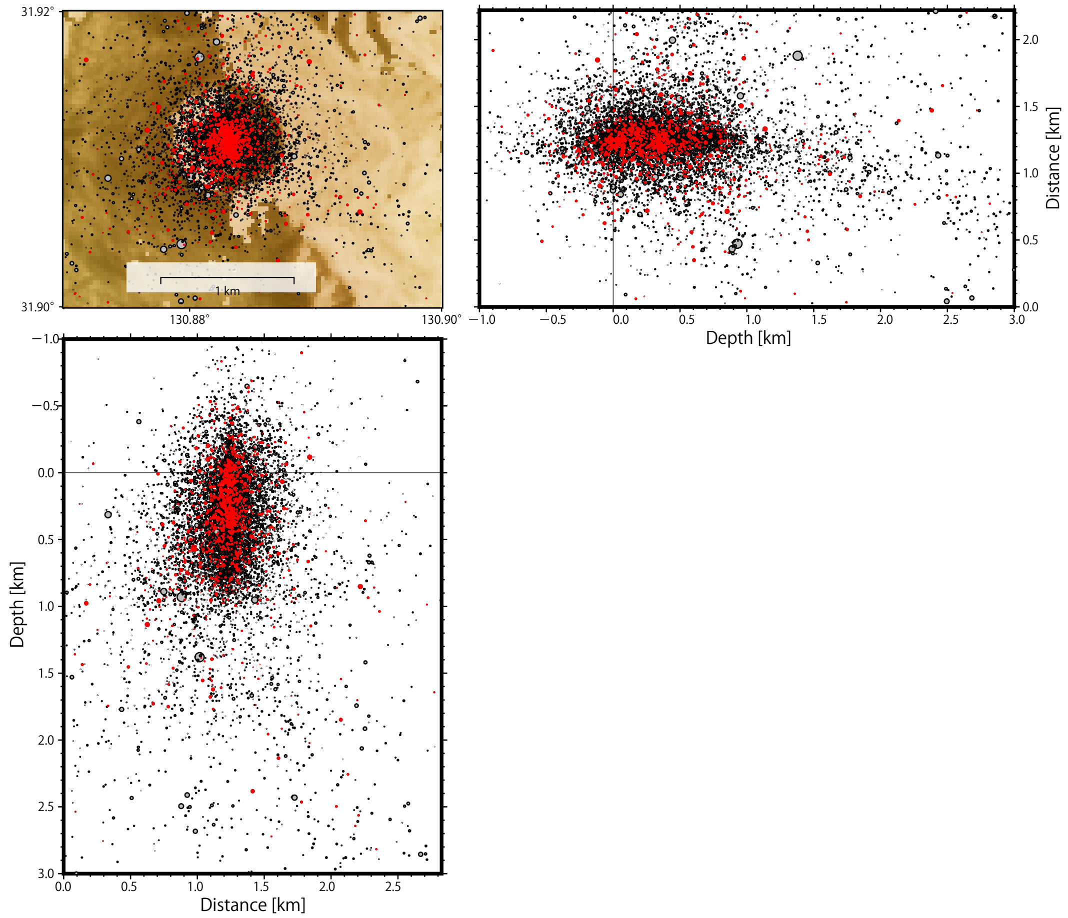

(b) Iwo-Yama

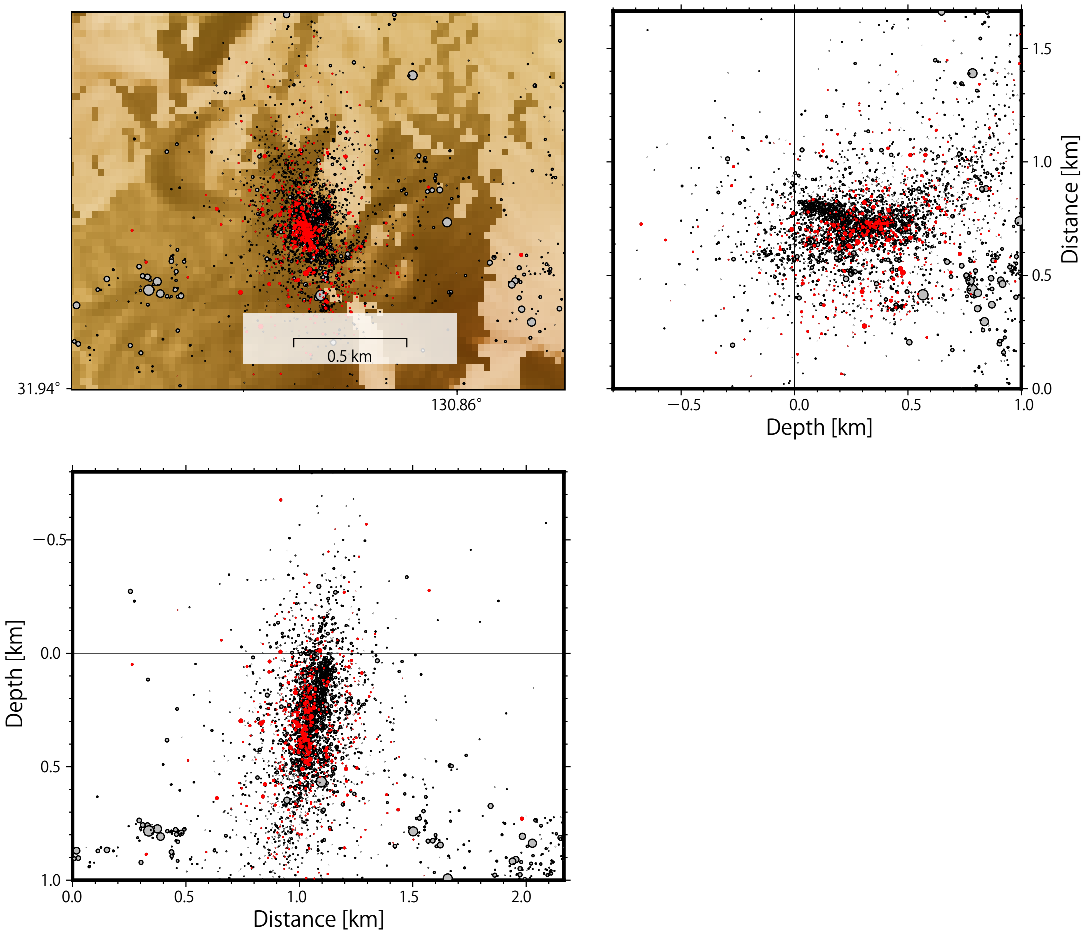

Figure4.

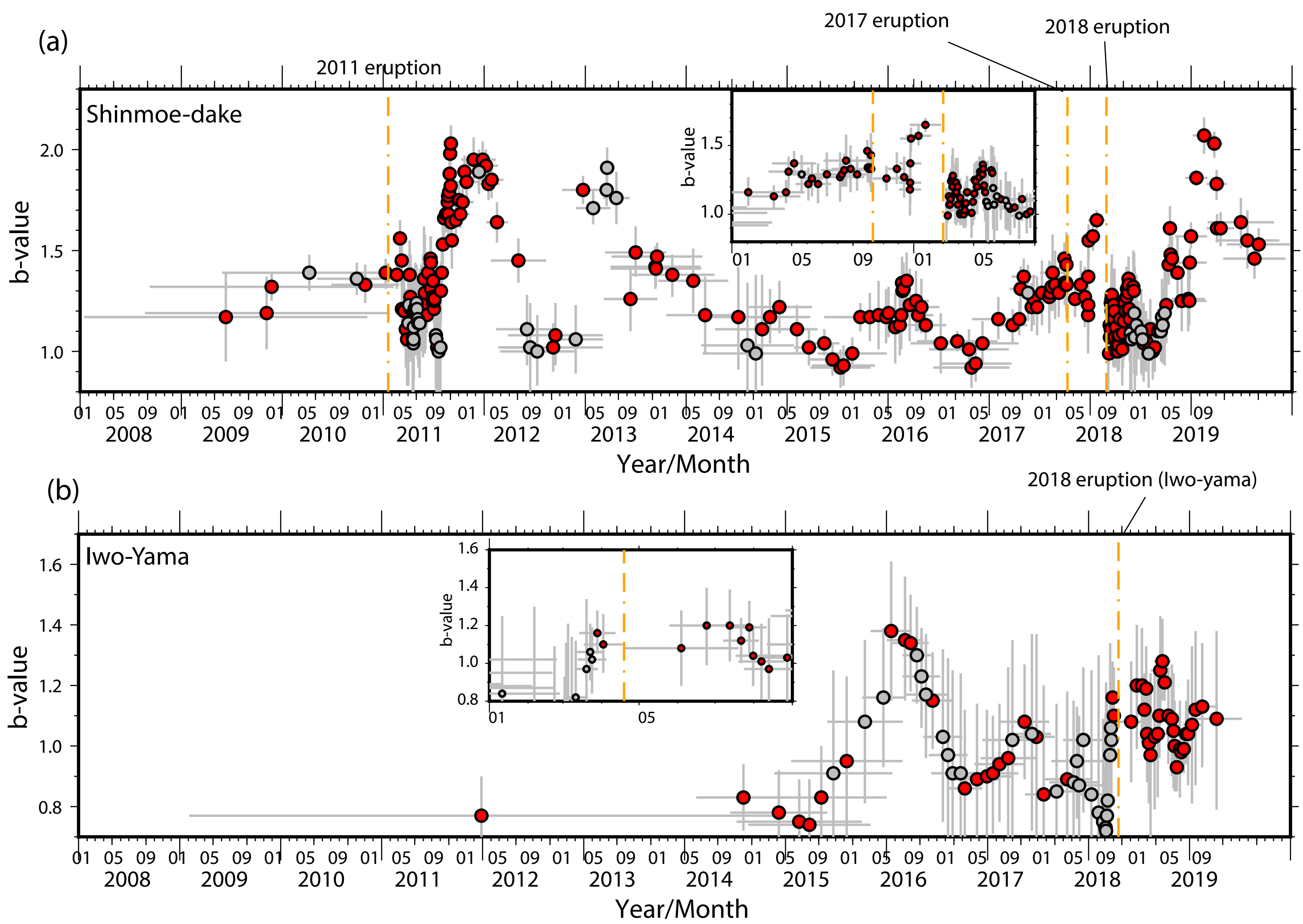

(a)
2011 eruption
2017 eruption
2018 eruption
Shinmoe-dake
b-value
Year/Month
(b)
2018 eruption (Iwo-yama)
Iwo-Yama
b-value
Year/Month